

K^0 - Σ^+ Photoproduction with SAPHIR

C. Bennhold^a, S. Goers^b, J. Barth^b, W. Braun^b, R. Burgwinkel^b, J. Ernst^c, K.H. Glander^b, J. Hannappel^b, N. Jöpen^b, H. Kalinowsky^c, U. Kirch^b, F. Klein^b, F.J. Kleing^e, E. Klempt^c, A. Kozela^e, R. Lawall^b, Zhenping Li^h, J. Link^c, T. Mart^{a,f}, D. Menze^b, W. Neuerburg^b, M. Paganetti^b, E. Paul^b, H. van Pee^c, R. Plötzke^c, M. Schumacher^d, W.J. Schwille^b, F. Smend^d, J. Smyrski^e, H.-N. Tran^d, M.Q. Tran^b, F. Wehnes^b, B. Wiegers^b, F.W. Wieland^b, J. Wißkirchen^b

^aCenter for Nuclear Studies, Department of Physics, The George Washington University, Washington DC 20052, USA

^bPhysikalisches Institut, Universität Bonn, 53115 Bonn, Germany

^cISKP, Universität Bonn, 53115 Bonn, Germany

^dII. Phys. Institut, Universität Göttingen, 37073 Göttingen, Germany

^eJagellonian University, Cracow, Poland

^fJurusan Fisika, FMIPA, Universitas Indonesia, Depok 16424, Indonesia

^gTJNAF, Newport News, VA 23606, USA

^hDepartment of Physics, University of Peking, Beijing, 100871, P.R. China

Preliminary results of the analysis of the reaction $\gamma + p \rightarrow K^0 + \Sigma^+$ are presented. We show the first measurement of the differential cross section and much improved data for the total cross section than previous data. The data are compared with model predictions from different isobar and quark models that give a good description of $\gamma + p \rightarrow K^+ + \Lambda$ and $\gamma + p \rightarrow K^+ + \Sigma^0$ data in the same energy range. None of the models yield an adequate description of the data at all energies.

1. PHYSICS WITH THE SAPHIR-DETECTOR

SAPHIR (Spectrometer Arrangement for PHoton Induced Reactions) [1] is a magnetic spectrometer setup at the 3.5 GeV electron accelerator ELSA in Bonn and is designed for the detection of multiparticle final states. The physics aim is the investigation of photon-induced reactions off protons and deuterons, especially the photoproduction of associated strangeness, of the lightest vector mesons ρ , ω and ϕ and of the pseudoscalar particles η and η' . With our experimental setup we are able to measure total and differential cross sections as well as hyperon polarizations. A goniometer setup for experiments with polarized photons is being tested and optimized. First results of $\gamma + p \rightarrow K^+ + \Lambda$ and $\gamma + p \rightarrow K^+ + \Sigma^0$ were published in Ref. [2].

The SAPHIR-detector is shown in Fig. 1. It uses a tagged photon beam and the data presented here have been taken with a tagging range of $(0.55 - 0.95) \cdot E$, where E is the energy of the electron beam from ELSA. The target cylinder, filled with liquid hydrogen or

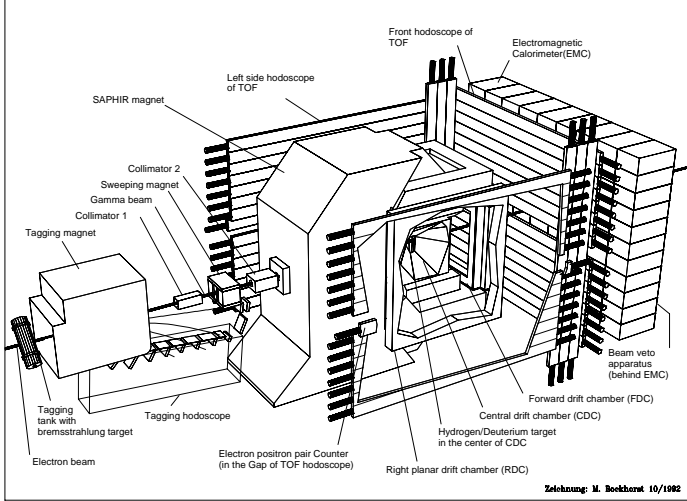


Figure 1.
The SAPHIR detector

deuterium, is located in the gap of a large magnet and is surrounded by a drift chamber system, consisting of a cylindrical central drift chamber and planar drift chambers in forward and sideward directions. They provide the track reconstruction and momentum measurement of the charged particles created in the target. A system of scintillator hodoscopes serves as trigger device and for the determination of particle masses via time-of-flight measurements. The electromagnetic calorimeter is currently in a test phase and will later be used for the identification of γ 's coming from hadron decays.

2. DATA REDUCTION AND ANALYSIS

The data presented here was taken at an electron energy of 1.7 GeV, i.e. we cover the photon energy range from threshold ($E_\gamma = 1.047$ GeV) to $E_\gamma = 1.6$ GeV [3]. Starting from three reconstructed tracks, the first step is to choose a subsystem of two tracks with positive and negative charge, with a common vertex and an invariant mass in the range of the K^0 mass. The measured 3-momenta of the π^+ and π^- (from K^0 decay) determine the momentum of the K^0 . Taking the calculated K^0 momentum and the measured energy of the incident γ , the missing mass at the primary vertex must be consistent with m_{Σ^+} . The missing Σ^+ momentum at the primary vertex is calculated using a kinematical fit with γ -energy and K^0 momentum as input. In the next step an iterative vertex fit determines the location of the primary vertex and the Σ^+ decay-vertex simultaneously. The identification of the Σ^+ decay channel ($\Sigma^+ \rightarrow p + \pi^0$ or $\Sigma^+ \rightarrow n + \pi^+$) is also obtained by a kinematical fit. The last step in the analysis is the separation from background reactions.

Figure 2 (A) shows the invariant mass distribution of the K^0 at the K^0 decay vertex, calculated from the measured π^+ and π^- tracks; Fig. 2 (B) shows the lifetime distribution of the Σ^+ obtained from reconstructed events.

3. COMPARISON BETWEEN THEORY AND EXPERIMENT

The measured differential cross section for the reaction $\gamma + p \rightarrow K^0 + \Sigma^+$ as a function of the kaon angle is shown in Fig. 3. Such data are presented here for the first time, the only previous data were total cross section data of poor statistics [4]. Since $K^0\Sigma^+$

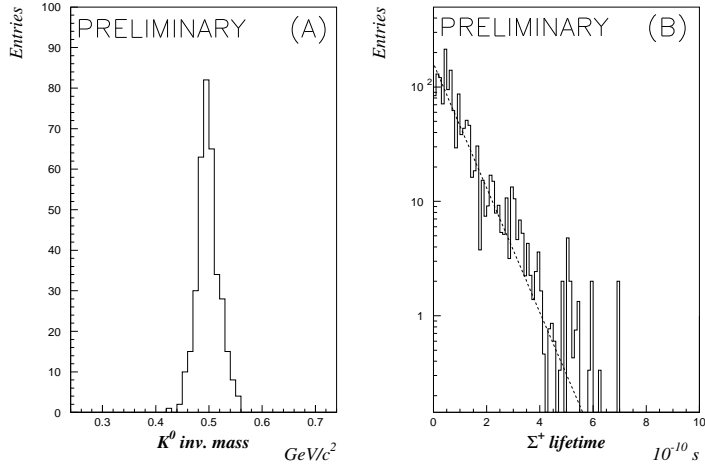


Figure 2.
 (A) K^0 invariant-mass distribution and
 (B) lifetime of the Σ^+ (dashed: PDB-value)

photoproduction is related to $K^+\Sigma^0$ production through simple isospin relations both processes should be described by the same model. Our data are compared with different isobar models which constitutes the most widely used method of analyzing these reactions [5–7]. In this framework, a number of s -, t - and u -channel resonances are included at tree level where unknown coupling constants are left as free parameters to be determined by the data. To eliminate the divergence of cross sections at higher energies several methods have been proposed: additional resonances, using reduced coupling constants, and absorptive factors. Ref. [5] has for the first time introduced a hadronic form factor at the $K\Lambda N$ and $K\Sigma N$ vertex. Multiplying the amplitude with an overall monopole form factor that depends on the momentum transfer t achieves a good overall fit to all photo- and electroproduction data of $K^+\Lambda$ and $K^+\Sigma^0$ with a cut-off around 700 MeV, while allowing the coupling constants to assume their SU(3) values. However, as shown in Fig. 3, this fit gives a prediction for $K^0\Sigma^+$ that is backward-peaked at higher energies while the data clearly exhibit forward peaking. Similar results are obtained from the quark model calculation of Ref. [8] that has fixed resonance couplings and therefore far fewer free parameters compared to isobar descriptions. Hadronic form factors are provided by the overlap of the quark wave functions. The quark model results shown here were performed in the exact $SU(3) \otimes O(3)$ limit, thus, quantitative agreement cannot be expected. The ChPT result of Ref. [10] gives an adequate description of the data at 1.075 GeV, however, due to its limited range of applicability it cannot be compared to data at higher energies.

While multiplying the whole amplitude with an overall form factor does preserve gauge invariance it represents a theoretically unjustified (though widely used) approach to include the finite hadron size since each tree level diagram should depend on a form factor that is a function of the corresponding off-shell variable. A naive implementation of this approach would lead to the violation of gauge invariance, however, using the procedure outlined in Ref. [9] allows gauge invariance to be restored. As shown in Fig. 3, this model predicts differential cross sections for $K^0\Sigma^+$ production that are now forward peaked, even though they overpredict the data by up to a factor of 3 at higher energies. The total cross section as a function of the photon energy, shown in Fig. 4, also cannot be reproduced in the isobar descriptions while the quark model gives the correct magnitude at higher energies.

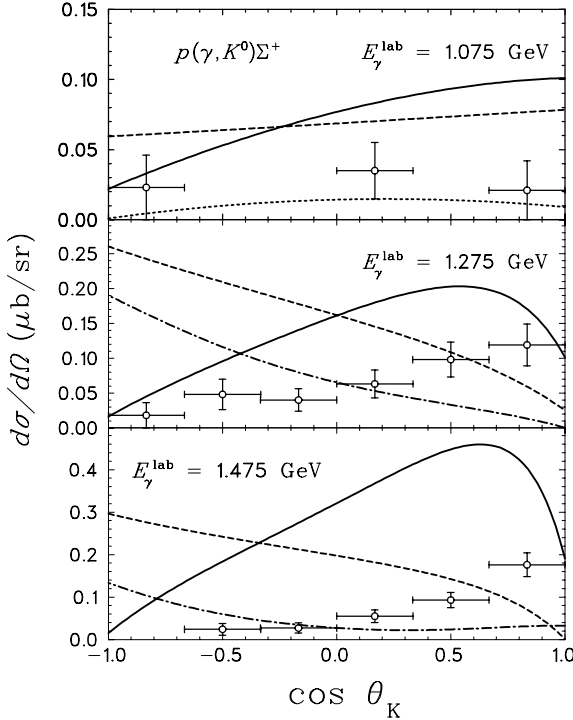


Figure 3. Differential cross sections for $p(\gamma, K^0)\Sigma^+$. The dashed (solid) curve shows an isobar model with an overall hadronic form factor [5] (includes the hadronic form factors according to Ohta [9]), while the dash-dotted (dotted) curve shows quark model [8] (ChPT [10]) calculation.

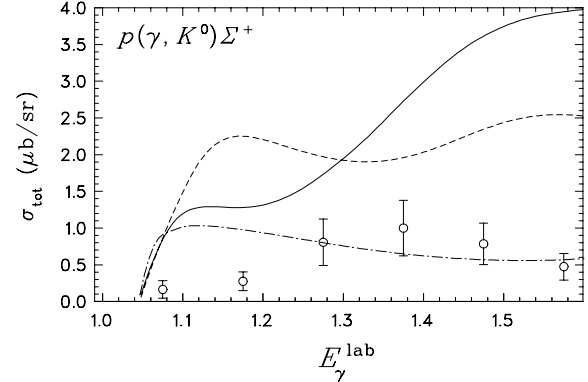


Figure 4. As in Fig. 3, but for the total cross section.

REFERENCES

1. W.J. Schwille *et al.*, Nucl. Instr. and Meth. A 344 (1994) 470.
2. SAPHIR collaboration, M. Bockhorst *et al.*, Z. Phys. C 63 (1994) 37.
3. S. Goers, dissertation, University of Bonn, in preparation.
4. ABBHHM-Collaboration, Phys. Rev. 188-2 (1969) 2060.
5. T. Mart and C. Bennhold, Few-Body Systems Suppl. 9 (1995) 369, T. Mart, Ph.D. Thesis, University of Mainz (1996), C. Bennhold, T. Mart, D. Kusno, Proc. of the TJ-NAF/INT workshop on N^* Physics, Seattle, WA, Sept. 9-13, 1996, (World-Scientific, 1997), p.166 (nucl-th/9703004).
6. J.C. David, C. Fayard, G.H. Lamot, and B. Saghai, Phys. Rev. C 53 (1996) 2613.
7. R.A. Williams, C.-R. Ji, and S.R. Cotanch, Phys. Rev. C 46 (1992) 1617.
8. Zhenping Li, Phys. Rev. C 54, (1996) R2171.
9. K. Ohta, Phys. Rev. C 40 (1989) 1335.
10. S. Steininger and U.G. Meissner, Phys. Lett. B 391 (1997) 446.